Control Engineering Practice 53 (2016) 124–138

Contents lists available at ScienceDirect

Control Engineering Practice

journal homepage: www.elsevier.com/locate/conengprac

Bridging the gap between the linear and nonlinear predictive control: Adaptations for efficient building climate control

Matej Pčolka [a,*], Eva Žáčeková [a,*], Rush Robinett [b], Sergej Čelikovský [c], Michael Šebek [a]

[a] Department of Control Engineering, Faculty of Electrical Engineering, Czech Technical University in Prague, Technická 2, 166 27 Praha 6, Czech Republic
[b] Mechanical Engineering-Engineering Mechanics, Michigan Technological University, United States
[c] Institute of Information Theory and Automation, Czech Academy of Sciences, Czech Republic

ARTICLE INFO

Article history:
Received 7 June 2015
Received in revised form
23 January 2016
Accepted 24 January 2016
Available online 5 February 2016

Keywords:
Model predictive control
Identification for control
Building climate control

ABSTRACT

The linear model predictive control which is frequently used for building climate control benefits from the fact that the resulting optimization task is convex (thus easily and quickly solvable). On the other hand, the nonlinear model predictive control enables the use of a more detailed nonlinear model and it takes advantage of the fact that it addresses the optimization task more directly, however, it requires a more computationally complex algorithm for solving the non-convex optimization problem. In this paper, the gap between the linear and the nonlinear one is bridged by introducing a predictive controller with linear time-dependent model. Making use of linear time-dependent model of the building, the newly proposed controller obtains predictions which are closer to reality than those of linear time invariant model, however, the computational complexity is still kept low since the optimization task remains convex. The concept of linear time-dependent predictive controller is verified on a set of numerical experiments performed using a high fidelity model created in a building simulation environment and compared to the previously mentioned alternatives. Furthermore, the model for the nonlinear variant is identified using an adaptation of the existing model predictive control relevant identification method and the optimization algorithm for the nonlinear predictive controller is adapted such that it can handle also restrictions on discrete-valued nature of the manipulated variables. The presented comparisons show that the current adaptations lead to more efficient building climate control.

1. Introduction

Presently, energy savings and reduction of energy consumption in buildings are some of the most challenging issues facing the engineering community. The reason is straightforward and the numbers speak for themselves – up to 40% of the total energy consumption can be owed to the building sector (Perez-Lombard, Ortiz, & Pout, 2008). More than half of this 40% is consumed by various building heating/cooling systems. Therefore, the recent significant emphasis on the energy savings in this area is right on target and can be observed in recent years. For example, the strategy of the European Union called "20–20–20" (European Economic & Social Committee, 2005) should be mentioned. Intended to be followed by all of Europe through the year 2020, this strategy aims at 20% reduction of the use of primary energy sources and production of the greenhouse gas emissions, and the renewable energy sources are expected to provide 20% of the consumed energy. With the clearly evident need for savings in the area of the building climate control, improvements can be found when considering the latest control techniques.

Model Predictive Control (MPC) is one of the most promising candidates for an energetically efficient control strategy (Pčolka, Žáčeková, Robinett, Čelikovský, & Šebek, 2014a, 2014b). This was also demonstrated within the framework of the Opticontrol project. One research team at ETH Zurich (Switzerland) showed via numerous simulations that using MPC instead of the classical control strategies achieves more than 16% savings (Gyalistras & Gwerder, 2010; Oldewurtel et al., 2010) depending on the building type. If one considers real operational conditions, these savings can be even higher when the MPC is modified appropriately for the conditions. This was shown by teams from Prague (Prívara, Široký, Ferkl, & Cigler, 2011; Žáčeková & Prívara, 2012 and UC Berkeley (Ma, Kelman, Daly, & Borrelli, 2012) where the actual cost savings were even better than the theoretical expectations (27% and 25% reduction of the energy consumption, respectively).

However, MPC suffers from several drawbacks including the complexity of the optimization routine and the need for a reliable mathematical model of the building. In order to be feasible and

* Corresponding authors.
E-mail addresses: matej.pcolka@fel.cvut.cz (M. Pčolka), eva.zacekova@fel.cvut.cz (E. Žáčeková), rdrobine@mtu.edu (R. Robinett), celikovs@utia.cas.cz (S. Čelikovský), sebekm1@fel.cvut.cz (M. Šebek).

http://dx.doi.org/10.1016/j.conengprac.2016.01.007
0967-0661/

computable, simplified formulations are often considered. Moreover, linear models are usually assumed and exploited by the optimizer. Therefore, in the majority of the MPC applications, the overall task is formulated as a linear/convex optimization problem easily solvable by the commonly available solvers for quadratic or semidefinite programming (Verhelst, Degrauwe, Logist, Van Impe, & Helsen, 2012; Prívara et al., 2011). Although being computationally favorable and able to find the global minimum in case of the convex formulation of the optimization task, their disadvantage is that they do not enable minimization of the nonlinear/nonconvex cost criteria and therefore, only certain approximation of the real cost paid for the control is optimized. Moreover, they resort to the optimization of either the setpoints or the energy delivered to the heating/cooling system while leaving all its distribution to the suboptimal low-level controllers which can lead to a significant loss of the optimality gained by the MPC.

In several recent works, the effort to take the nonlinearities (caused either by the dynamical behavior of the building or by the control requirements formulation) into account within the optimization task can be found (Ma et al., 2012, 2011). In this paper, we discuss both possibilities for the zone temperature control (the linear and the nonlinear MPC) and moreover, we bridge the two banks of the gap between the nonlinear and the linear variant of the MPC by introducing linear model that changes in time. Such model can describe the building dynamics in a more reliable and flexible way than the original linear model while it still keeps the low complexity of the optimization task (since with the linear model, the optimization task to be solved remains convex). The way of obtaining a time-varying model is described and the results of the linear predictive controller with linear model that changes in time are compared with the results of the original (linear and nonlinear) MPCs.

It should be mentioned that a good predictive controller relies on a good system dynamics predictor and therefore, we focus on the identification of such reliable multi-step predictors as well. The MPC employs optimization over certain given prediction horizon and this fact should be taken into consideration also in the design of the identification procedure. Unlike the commonly used identification methods (PEM, Ljung, 1999) which provide models that are able to predict well only over short horizons, the methods based on minimization of multi-step prediction errors (MRI – model predictive control relevant identification, Laurí, Salcedo, Garcia-Nieto, & Martínez, 2010) offer models with more attractive prediction properties. Therefore, we exploit the MRI for identification of both linear and nonlinear models. While several published works deal with application of MRI for estimation of parameters of linear models (Chi, Fei, Zhao, Zhao, & Liang, 2014; Shook, Mohtadi, & Shah, 1991; Zhao, Zhu, & Patwardhan, 2014), no extension, to the best knowledge of the authors of this paper, has been provided for estimation of parameters of *nonlinear* models. Moreover, even the linear version of MRI in the literature is usually validated only on simple artificial examples. On the other hand, this paper presents application of both the linear and the newly proposed nonlinear MRI versions on much more complex and realistic example of building model identification.

Furthermore, a very important practical aspect of the building temperature control is addressed in this work as well. In real-life building applications, water pumps are a crucial part of the actuators used to manipulate the optimized input variables. These water pumps possess nonlinear output dynamics where the amount of mass flow rate which can be provided by the pump is often quantized. Therefore, the achievable water mass flow rates belong to a countable set of discrete values rather than to a continuous interval. The appropriately designed control algorithm should take this information properly into account. This can be performed in several ways: (1) mixed-integer programming techniques can be employed, (2) additional postprocessing after the calculation of the optimal inputs can be applied, or (3) the (originally continuous-valued) optimization procedure itself can be adapted such that discrete-valued input profiles are obtained.

First of all, the mixed-integer programming approach is the most suitable one in case that one of the manipulated variables should belong to countable set of discrete values. However, the mixed-integer programming problems are known to be NP-hard (Bussieck & Vigerske, 2010; Lenstra, 1983; Pancanti, Leonardi, Pallottino, & Bicchi, 2002) and their solution using mixed-integer programming solvers requires massive computational power. Furthermore, the majority of reliable currently available mixed-integer solvers able to handle nonlinear system description/nonlinear optimization criterion are not free for industrial use. Since the computational burden caused by solving the mixed-integer programming task is huge and it is in direct opposite to the extensive effort to simplify the control schemes and systems used in buildings, this direction is not suitable. Instead of formulating the building temperature control problem as a mixed-integer programming task, the other two mentioned options (additional postprocessing and adaptation of the continuous-valued optimization procedure) are elaborated in the current paper.

The paper is organized as follows: Section 2 illustrates the problem of the building climate control on a simple example. Both the building and the heat delivery system description are provided. Furthermore, control performance criterion, comfort requirements and restrictions are introduced. In Section 3, the models supplying predictions to the model-based controllers are described. The nonlinear model is derived in Section 3.1 based on the thermodynamics while for the linear model, the assumed simplifications are presented in Section 3.2. The linear time-varying model is presented in Section 3.3. A new approach to estimating parameters of the nonlinear model with respect to the multi-step prediction error minimization criterion proposed in Section 3.4. Two alternative versions of this approach are presented which are some of the main contributions of this paper. All models are verified on the data set obtained from TRNSYS environment and their results are discussed. Section 4 describes the controllers including the low level re-calculation (for the linear MPC) and the nonlinear optimization routine (for the nonlinear MPC). In order to address the discrete-valued nature of part of the considered actuators, the nonlinear MPC optimization routine is changed in two ways: either a naive additional post-processing is employed or the *mid-processing* iteration (which is another main contribution of this paper) is incorporated into the routine. In Section 5, building behaviors of all proposed controllers are investigated and their results are presented and examined. Section 6 draws conclusion of the paper.

2. Problem formulation

In this section, the description of the building, constraints and the evaluative performance criterion are formulated.

2.1. Building of interest

The building under our investigation is a simple medium weight one-zone building modeled in the TRNSYS16 (University of Wisconsin-Madison, 1979) environment, which is a high fidelity simulation software package widely accepted by the civil engineering community as a reliable tool for simulating the building behavior.

The building considered in this paper is a medium sized one with a size of $5 \times 5 \times 3$ m and a single-glazed window (3.75 m^2) placed in the south-oriented wall. The Heating, Ventilation and Air

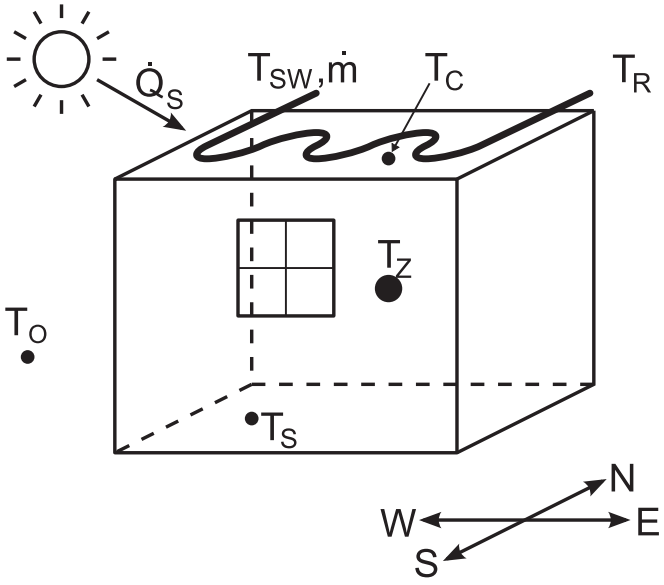

Fig. 1. A scheme of the modeled building.

Conditioning (HVAC) system used in the building is of the so-called active layer type. Technically, the HVAC system consists of TABS (thermally activated building system) – a set of metal pipes encapsulated into the ceiling distributing the supply water which then enables thermal exchange with the concrete core of the modeled building consequently heating the air in the room. This configuration corresponds to the commonly used building heating system in the Czech Republic. Ambient environmental conditions (ambient temperature, ambient air relative humidity, solar radiation intensity and others) are simulated using TRNSYS Type15 with the yearly weather profile corresponding to Prague, Czech Republic.

Fig. 1 shows a sketch of the building HVAC system configuration, the "building" variables and the environment variables. Regarding the building inner variables, four of them are considered to be available – zone temperature T_Z, ceiling temperature T_C, temperature of the return water T_R and temperature of the south-oriented wall T_S. From the environmental influences, solar radiation $\dot{Q}_S$ and outside-air temperature T_O are taken into account as disturbances while the supply water temperature T_{SW} and the mass flow rate of the supply water $\dot{m}$ are the controlled input variables. The TRNSYS model in this configuration offers a good numerical test-bed to compare the control approaches, and the results obtained with this model can be generalized without any loss of objectivity.

The next step is to describe the heat distribution system. In the application presented in this paper, the configuration of the heating system as shown in Fig. 2 is considered. Clearly, the storage tank plays a key role as the sole heat supplier in this system. In fact, having obtained the requirements for the supply water temperature T_{SW} and the supply water mass flow rate $\dot{m}$, these two values are "mixed" using the return water with the temperature T_R flowing into the building inlet pipe through the side-pipe at the mass flow rate $\dot{m}_s$ and the water from the storage tank which is kept at certain constant value T_{St} (in this paper, $T_{St} = 60\,^{\circ}\mathrm{C}$ is considered) and can be withdrawn from the tank at mass flow rate $\dot{m}_{St}$. Based on this, the following set of equations can be written for the upper three-way valve:

$$\begin{aligned} \dot{m}T_{SW} &= \dot{m}_{St}T_{St} + \dot{m}_S T_R \\ \dot{m} &= \dot{m}_{St} + \dot{m}_S. \end{aligned} \tag{1}$$

which can be further rewritten into an expression for the

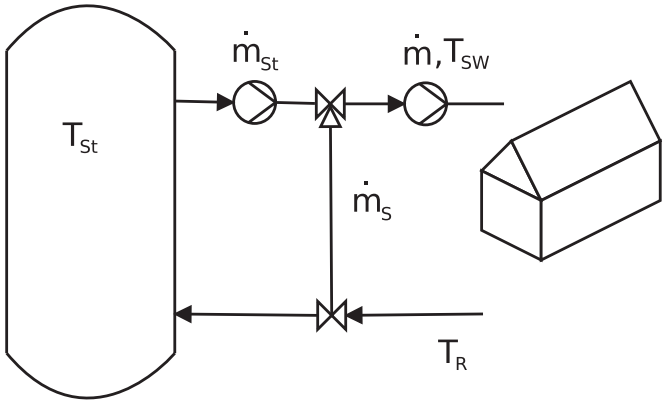

Fig. 2. A scheme of heat distribution system.

calculation of the storage water mass flow rate,

$$\dot{m}_{St} = \dot{m}\frac{(T_{SW} - T_R)}{(T_{St} - T_R)}. \tag{2}$$

Having the return water temperature values at disposal and extracting the storage water with the temperature of T_{St} at the mass flow rate $\dot{m}_{St}$, both the supply water temperature and supply water mass flow rate related to the heating requirements can be achieved.

2.2. Control performance requirements

Considering the building climate control, one of the most important tasks is to ensure the required thermal comfort which is specified by a pre-defined admissible range of temperatures related to the way of use of the building (office building, factory, residential building, etc.). Under the weather conditions of middle Europe with quite low average temperatures where heating is required for more than half of year, the thermal comfort satisfaction requirement can be further simplified such that the zone temperature is bounded only from below. Since an office building with regular time schedule is considered, the lowest admissible zone temperature $T_Z^{min}(t)$ whose violation will be penalized is defined as a function of working hours as

$$T_Z^{min}(t) = \begin{cases} 22\,^{\circ}\mathrm{C} & \text{from 8 a. m. to 6 p. m.,} \\ 20\,^{\circ}\mathrm{C} & \text{otherwise.} \end{cases} \tag{3}$$

Then, the thermal comfort violation is expressed as

$$CV(t) = \max(0, T_Z^{min}(t) - T_Z(t)). \tag{4}$$

Besides the comfort violation $CV(t)$, the price paid for the operation of the building is penalized in the cost criterion as well. Coming out of the considered structure of the building and its energy supply system, the monetary cost includes the price for the consumed hot water and the electricity needed to operate the two water pumps. While the hot water price P_W is considered constant (see Table 1), the electricity price $P_E(t)$ which applies to the operation of the supply and storage water pumps is piece-wise constant and similar to the lowest admissible zone temperature

Table 1
List of the specific parameters.

T_Z^{min} (°C)	22/20	P_W (–)	2.6199
HT (€/kWh)	0.1168	α_0 (–)	9
LT (€/kWh)	0.0502	α_1 (–)	9.25×10^{-3}
T_{St} (°C)	60	α_2 (–)	1.875×10^{-6}
$[\underline{\dot{m}}, \overline{\dot{m}}]$	[15,60]	ΔT (°C)	5

profile, it depends on the working hours as follows:

$$P_E(t) = \begin{cases} HT & \text{from 8 a. m. to 6 p. m.,} \\ LT & \text{otherwise.} \end{cases} \quad (5)$$

In order to bring the presented case study closer to reality, the values of high and low tariff (*HT* and *LT*) have been chosen in accordance with the real prices approved by the Regulatory Office for Network Industries of Slovak Republic (R.O. for Network Industries, 2011). The exact values of *HT* and *LT* in €/kWh are listed in Table 1.

Thus, the overall performance criterion over a time interval $\langle t_1, t_2 \rangle$ is formulated as

$$J = \int_{t_1}^{t_2} \omega CV(t)\,\mathrm{d}t + \int_{t_1}^{t_2} \left(P_E(t)(P_C(\dot{m}) + P_C(\dot{m}_{St})) + P_W \dot{m}_{St}\right)\mathrm{d}t. \quad (6)$$

Here, ω is the virtual price for the comfort violation $CV(t)$ which is defined by Eq. (4) and $P_W \dot{m}_{St}$ represents the cost paid for the consumed hot water. Time-varying electricity price is expressed as a function of time by Eq. (5) and the power consumptions of the water pumps corresponding to $\dot{m}$ and $\dot{m}_{St}$ can be calculated as a quadratic function of the particular mass flow rate,

$$P_C(\dot{m}) = \alpha_0 + \alpha_1 \dot{m} + \alpha_2 \dot{m}^2,$$
$$P_C(\dot{m}_{St}) = \alpha_0 + \alpha_1 \dot{m}_{St} + \alpha_2 \dot{m}_{St}^2. \quad (7)$$

The parameters $\alpha_{0,1,2}$ are listed in Table 1.

Let us note that since the criterion (6) specifies the control requirements for the control of a building in a very compact form, all considered controllers will be evaluated and compared according to this criterion.

2.3. Constraints

In order to ensure proper functionality of the heat distribution system depicted in Fig. 2, the following technical constraints imposed on the manipulated variables need to be taken into account.

First of all, the constraints on mass flow rates which can be achieved by both the supply water pump and storage water tank pump need to be respected. The upper bound of the mass flow rates is given by the maximal power of the considered pumps. Technically, the lower bound on the supply water mass flow rate $\underline{\dot{m}}$ and storage tank mass flow rate $\underline{\dot{m}}_{St}$ is zero, however, the supply water pump is required to always maintain some nonzero supply water mass flow rate. To prevent the supply water pump from damage resulting from water overpressure potentially caused by the storage tank pump, the storage tank mass flow rate must never exceed the supply water mass flow rate. Due to this, the mass flow rate of the supply water and the storage tank mass flow rate are bound together by the relation $\dot{m}_{St} \le \dot{m}$. The last mass flow rate constraint results from a common feature of the water pumps that are very often multi-valued and cannot set the mass flow rate with arbitrarily small sensitivity. Therefore, the mass flow rate values must belong to a countable admissible set of discrete values.

The second group of constraints is imposed on the supply water temperature. Since the storage tank is the only source of hot water and no additional heater that could increase the water temperature to values higher than T_{St} is considered, it is obvious that the highest required supply water temperature must be lower than or equal to storage water temperature. However, the heat losses caused by the transportation of the storage water should be also reflected and therefore, it is more realistic to consider the upper constraint for the supply water temperature to be several degrees lower than the storage water temperature. Last of all, let us note that a situation which requires a value of T_{SW} to be lower than the return water temperature T_R would mean negative storage water mass flow rate $\dot{m}_{St}$, which can not be practically realized. On the other hand, it is also obvious that such T_{SW} requirement really cannot be satisfied as only the hot water storage is considered in this configuration. With no cold water storage neither water chiller provided, the temperature of the supply water cannot be decreased below the return water temperature and the active cooling mode is not allowed.

Since the storage water mass flow rate is not an independent variable and is uniquely given by the supply water mass flow rate $\dot{m}$ and supply water temperature T_{SW}, the constraints for storage water mass flow rate can be omitted. To sum up, the above mentioned technical constraints are mathematically formulated as follows:

$$\underline{\dot{m}} \le \dot{m} \le \overline{\dot{m}}$$
$$\dot{m} \in \dot{M}_{\mathrm{adm}} = \{\dot{m}_{\mathrm{a}} | \dot{m}_{\mathrm{a}} = a \times q_{st},\ a \in \mathbb{Z}\},$$
$$\max\{T_R, \underline{T}_{SW}\} \le T_{SW} \le T_{St} - \Delta T. \quad (8)$$

Parameters $\underline{\dot{m}}$, $\overline{\dot{m}}$ and ΔT are provided in Table 1. Several different values of quantization steps q_{st} were considered in this work and their exact values are specified later.

3. Modeling and identification

In this section, the derivation of models for the particular variants of the MPC (being one of the crucial part of the whole control approach) is described and explained. A special emphasis is put on explanation and description of Model Predictive Control Relevant Identification (MRI) approach, the identification procedure providing mathematical models with good prediction behavior on wider range of prediction horizons.

3.1. Nonlinear model (NM)

In the current paper, the methodology that is widely used for modeling of heat transfer effects in buildings (ASHRAE, 2009; Barták, 2010; Lienhard, 2013) is followed. As explained in the dedicated literature, several physical phenomena need to be considered to obtain an appropriate structure reliably describing the building behavior. The most crucial aspects influencing the thermodynamics within the inspected zone are:

1. *Convection from walls*: This phenomenon occurs when fluid (in this case the zone air) moves along the body (wall) with different surface temperature. It affects both the heated wall T_C and the unheated wall T_S and the zone temperature T_Z. Derived from the well known Newton's cooling law, the heat flux $q_{W,\mathrm{conv}}$ caused by convection can be expressed as

   $$q_{W,\mathrm{conv}} = h_{W,\mathrm{conv}}(T_W - T_Z).$$

   In this expression, $h_{W,\mathrm{conv}}$ denotes the convection heat transfer coefficient and T_W refers to temperature of one of the considered walls, i.e. T_C or T_S.
   In case that the fluid is externally forced to move, the convection heat transfer coefficient $h_{W,\mathrm{conv}}$ is independent of the temperature difference $T_W - T_Z$. However, in case that the fluid motion is caused solely by buoyant forces arisen from different temperatures of the fluid and the body (and thus temperature-dependent density of the fluid) and the gravitational effects, the convection heat transfer coefficient $h_{W,\mathrm{conv}}$ is expressed as a function of this temperature difference (ASHRAE, 2009; Lienhard, 2013). A common and empirically proven choice is to express the convection heat transfer coefficient $h_{W,\mathrm{conv}}$ as a weak function of the temperature difference $\Delta T = T_W - T_Z$, typically $h_{W,\mathrm{conv}} \propto |\Delta T^{1/4}|$ or $h_{W,\mathrm{conv}} \propto |\Delta T^{1/3}|$ (Lienhard, 2013; Zmrhal & Drkal, 2006). Based on the technical specification of

the building examined in this paper (absence of the ventilation fan), the forced convection is neglected and the convection heat transfer coefficient is in accordance with ASHRAE (2009), Barták (2010), and Lienhard (2013) modeled as

$$h_{W,\mathrm{conv}} = \overline{h}_{W,\mathrm{conv}} \left| T_W - T_Z \right|^{\frac{1}{3}},$$

where $\overline{h}_{W,\mathrm{conv}}$ accounts also for influence of the surface area of the convecting wall $A_{W,\mathrm{conv}}$. Then, the convection heat flux $q_{W,\mathrm{conv}}$ from particular wall can be summarized as

$$q_{W,\mathrm{conv}} = \overline{h}_W \left| T_W - T_Z \right|^{\frac{1}{3}} (T_W - T_Z). \tag{9}$$

2. *Mutual interactions of the walls*: Out of the three possible heat transfer phenomena – conduction, radiation and convection –, the first two might apply when inspecting the mutual interactions between the considered walls (ASHRAE, 2009; Lienhard, 2013). Conduction heat flux q_{cond} occurs due to the presence of common edges and vertices of the walls and being the simpler one, it is expressed by a formula resembling Newton's cooling law (Balmer, 2010; Lienhard, 2013),

$$q_{W,\mathrm{cond}} = h_{\mathrm{cond}} (T_S - T_C).$$

Here, the conduction heat transfer coefficient $h_{W,\mathrm{cond}}$ is proportional to the surface area of the walls and inversely proportional to the distance between the points at which the temperatures T_C and T_S are provided.
Regarding the radiation, the well known Stefan–Boltzmann law applies:

$$q_{\mathrm{rad}} = h_{\mathrm{rad}} (T_S^4 - T_C^4),$$

with h_{rad} embracing (besides the effect of the Stefan–Boltzmann constant) various influences such as *view factor* between the two irradiating objects, emissivity/absorptivity and the surface area (Balmer, 2010). In case that the temperature difference between the two objects is relatively small (which holds true also for the heated and unheated wall temperatures), radiation heat flux q_{rad} can be with sufficient accuracy approximated by a linear function of the temperature difference,

$$q_{\mathrm{rad}} \approx \overline{q}_{\mathrm{rad}} = \overline{h}_{\mathrm{rad}} (T_S - T_C)$$

and the joint conduction/radiation heat flux can be then expressed as

$$q_{\mathrm{cd,rd}} = q_{W,\mathrm{cond}} + \overline{q}_{\mathrm{rad}} = h_{\mathrm{cd,rd}} (T_S - T_C). \tag{10}$$

3. *Effects of ambient environment*: Here, influences of solar radiation and ambient temperature are considered. The values of the first of them (solar radiation) are provided in terms of the corresponding heat flux and therefore, no further derivations are necessary, $q_{\mathrm{sol}} = \dot{Q}_S$. The latter one is assumed to be "measured" on the outer surface of the unheated wall and is assumed to vary only negligibly across the wall surface. Then, the heat flux resulting from the different inner and outer surface temperatures of the wall is described in terms of conduction through the wall as

$$q_O = h_{O,\mathrm{cond}} (T_O - T_S). \tag{11}$$

Since the heated wall contains metal piping filled with hot supply water, the effect of the ambient temperature T_O on the temperature T_C of its inner surface is neglected.
Due to the presence of the window and possible associated gaps and interstices, the ambient temperature is assumed to directly influence the zone temperature according to the following expression:

$$q_{O,Z} = h_{O,Z} (T_O - T_Z), \tag{12}$$

where the heat transfer coefficient $h_{O,Z}$ reflects all the above mentioned window-related leakage effects.

4. *Thermal energy supplied by the manipulated variables*: In the currently presented case, this energy is provided by the hot supply water of the temperature T_{SW} circulating at mass flow rate $\dot{m}$ in the metal piping encapsulated in the concrete core of the building. The thermal energy that is transferred from the supply water into the concrete core can be quantified as follows:

$$q_{\mathrm{in}} = c_w \dot{m} (T_{SW} - T_R). \tag{13}$$

Furthermore, based on the low thermal resistivity of the metals, it is assumed that the metal piping in which the water circulates has temperature T_P only negligibly different from the return water, $T_P \approx T_R$. Therefore, the return water temperature can be used for expression of the conductive heat transfer from the concrete core to the heated wall surface,

$$q_{R,\mathrm{cond}} = h_{R,\mathrm{cond}} (T_R - T_C), \tag{14}$$

with the heat transfer coefficient $h_{R,\mathrm{cond}}$ covering the effects of the different piping and wall materials and the distance from the water piping to the heated wall surface.

Based on this, thermodynamics of each of the considered inner variables of the building can be summarized:

- dynamics of the zone temperature T_Z is positively influenced by the convection from both considered walls and the heat flux coming from the ambient environment. Furthermore, the zone temperature is also increased due to the presence of solar radiation entering the room directly through the window,

$$\frac{\mathrm{d}T_Z}{\mathrm{d}t} \propto q_{C,\mathrm{conv}}, \quad \frac{\mathrm{d}T_Z}{\mathrm{d}t} \propto q_{S,\mathrm{conv}}, \quad \frac{\mathrm{d}T_Z}{\mathrm{d}t} \propto q_{O,Z}, \quad \frac{\mathrm{d}T_Z}{\mathrm{d}t} \propto q_{\mathrm{sol}}. \tag{15}$$

- heated wall surface temperature T_C is decreased by the amount of heat that is transferred into the zone air via convection while it is increased by the heat resulting from mutual interaction with the unheated wall and also by the heat transferred from heated supply water piping,

$$\frac{\mathrm{d}T_C}{\mathrm{d}t} \propto -q_{C,\mathrm{conv}}, \quad \frac{\mathrm{d}T_C}{\mathrm{d}t} \propto q_{\mathrm{cd,rd}}, \quad \frac{\mathrm{d}T_C}{\mathrm{d}t} \propto q_{R,\mathrm{cond}}. \tag{16}$$

- similar to the heated wall, the unheated wall is cooled down by the convection into the zone air. Moreover, the unheated wall surface temperature T_S decreases due to the thermal exchange with the heated wall while it is increased due to the effects of the ambient environment (ambient temperature T_O and solar radiation q_{sol}),

$$\frac{\mathrm{d}T_S}{\mathrm{d}t} \propto -q_{S,\mathrm{conv}}, \quad \frac{\mathrm{d}T_S}{\mathrm{d}t} \propto -q_{\mathrm{cd,rd}}, \quad \frac{\mathrm{d}T_S}{\mathrm{d}t} \propto q_O, \quad \frac{\mathrm{d}T_S}{\mathrm{d}t} \propto q_{\mathrm{sol}}. \tag{17}$$

- finally, the return water temperature T_R is affected by the supplied thermal energy and further heat transfer with the surface of the heated wall,

$$\frac{\mathrm{d}T_R}{\mathrm{d}t} \propto -q_{R,\mathrm{cond}}, \quad \frac{\mathrm{d}T_R}{\mathrm{d}t} \propto q_{\mathrm{in}} \tag{18}$$

For further use in a mathematical model, all the building inner variables are considered as the state variables of the mathematical model of the building thermodynamics, $x = [T_Z, T_C, T_S, T_R]$. Moreover, inputs $u = [T_{SW}, \dot{m}]$ stand for the manipulated variables being supply water temperature and the mass flow rate of the supply water and $d = [T_O, q_{\mathrm{sol}}]$ correspond to the predictable

disturbances, namely the temperature of the ambient environment and the solar radiation. Then, the above mentioned phenomena described by Eqs. (15)–(18) are captured by the following set of differential equations:

$$\begin{aligned}
\dot{x}_1 &= \overline{p}_1\left|x_2 - x_1\right|^{\frac{1}{3}}(x_2 - x_1) + \overline{p}_2\left|x_3 - x_1\right|^{\frac{1}{3}}(x_3 - x_1) + \overline{p}_3(d_1 - x_1) + \overline{p}_4 d_2\\
\dot{x}_2 &= -\overline{p}_5\left|x_2 - x_1\right|^{\frac{1}{3}}(x_2 - x_1) + \overline{p}_6(x_3 - x_2) + \overline{p}_7(x_4 - x_2)\\
\dot{x}_3 &= -\overline{p}_8\left|x_3 - x_1\right|^{\frac{1}{3}}(x_3 - x_1) - \overline{p}_9(x_3 - x_2) + \overline{p}_{10}(d_1 - x_3) + \overline{p}_{11} d_2\\
\dot{x}_4 &= -\overline{p}_{12}(x_4 - x_2) + \overline{p}_{13} u_2(u_1 - x_4).
\end{aligned} \tag{19}$$

To ensure admissible computational complexity of the predictive controller exploiting the nonlinear model, the structure (19) was discretized using Euler discretization method considering fixed a priori known sampling time t_s (Stetter, 1973). In this paper, $t_s = 15$ min is considered. The discretization procedure results in a series of difference equations expressing the one-step predictions of the system behavior,

$$\begin{aligned}
x_{1,k+1} &= x_{1,k} + p_1\left|x_{2,k} - x_{1,k}\right|^{\frac{1}{3}}(x_{2,k} - x_{1,k}) + p_2\left|x_{3,k} - x_{1,k}\right|^{\frac{1}{3}}(x_{3,k} - x_{1,k})\\
&\quad + p_3(d_{1,k} - x_{1,k}) + p_4 d_{2,k}\\
x_{2,k+1} &= x_{2,k} - p_5\left|x_{2,k} - x_{1,k}\right|^{\frac{1}{3}}(x_{2,k} - x_{1,k}) + p_6(x_{3,k} - x_{2,k}) + p_7(x_{4,k} - x_{2,k})\\
x_{3,k+1} &= x_{3,k} - p_8\left|x_{3,k} - x_{1,k}\right|^{\frac{1}{3}}(x_{3,k} - x_{1,k}) - p_9(x_{3,k} - x_{2,k})\\
&\quad + p_{10}(d_{1,k} - x_{3,k}) + p_{11} d_{2,k}\\
x_{4,k+1} &= x_{4,k} - p_{12}(x_{4,k} - x_{2,k}) + p_{13} u_{2,k}(u_{1,k} - x_{4,k}),
\end{aligned} \tag{20}$$

which are more suitable for implementation of the predictive controller than the continuous-time model (19). To obtain estimates of the parameters p of the discretized structure (20), MRI approach (whose explanation is provided later in this Section) belonging to advanced identification techniques was employed.[1]

3.2. Linear model (LM)

In order to simplify the model (19), let us adopt the assumption that the cubic roots of the temperature differences related to the heat convection are constant over the whole range of the operating points of the building. This simplifies the nonlinear terms as follows:

$$p|x_i - x_j|(x_i - x_j)^{\frac{1}{3}} \approx a(x_i - x_j). \tag{21}$$

Furthermore, $q_{\text{in}} = c_w \dot{m}(T_{SW} - T_R)$ is assumed to be the control input instead of the pair $\dot{m}$ and T_{SW}. Based on these assumptions, the linear version of the model Eq. (20) can be summarized as a discrete-time state space model as follows:

$$x_{k+1} = Ax_k + Bu_k + B_d d_k \tag{22}$$

with the state matrices having the following structure:

$$A = \begin{bmatrix} a_1 & a_2 & a_3 & 0\\ a_5 & a_6 & a_8 & a_7\\ a_9 & a_{10} & a_{11} & 0\\ 0 & a_{12} & 0 & a_{13} \end{bmatrix}, \quad B = \begin{bmatrix} 0\\ 0\\ 0\\ b \end{bmatrix}, \quad B_d = \begin{bmatrix} b_{d1} & b_{d2}\\ 0 & 0\\ b_{d3} & b_{d4}\\ 0 & 0 \end{bmatrix}. \tag{23}$$

In this model, state and disturbance variables correspond to the previously mentioned ones and $u = q_{\text{in}}$ refers to the optimized input. The sampling period of the system has been chosen as $t_s = 15$ min. The model parameters a, b, b_d have been estimated by a multistep prediction error minimization procedure (MRI). For further details on this method, the readers are referred to Žáčeková & Prívara (2012).

3.3. Switched linearly approximated model (SLM)

The main idea of this approach is that for a combination of inputs u, disturbances d and state variables x, a linear time-varying approximation of model (20) can be found by replacing particular nonlinearities with time-varying terms. In case of a building, this approach is even more natural and expected as the nonlinear mathematical description of the building contains terms depending on the differences between two state variables, namely $p\left|x_i - x_j\right|^{\frac{1}{3}}(x_i - x_j)$ which are likely to vary much less than the temperatures themselves. As an opposite to the linear models described earlier where the nonlinear terms are linearized "before the identification" and having the gathered data at disposal, parameters of linear time invariant model are estimated considering the purely linear character of the model, in this case, the nonlinear model is identified off-line and using its parameters, the nonlinearities are continuously approximated on-line depending on the actual values of the chosen auxiliary variables which leads to a time-varying linear model.

In order to get rid of the nonlinear terms coupling the states, let us propose an approximation procedure based on the auxiliary variables as follows.

Let us introduce two auxiliary variables, $\delta_{x_{1,2},k}$ and $\delta_{x_{1,3},k}$ defined such that

$$\begin{aligned}
\delta_{x_{1,2},k} &= \sqrt[3]{|x_{2,k_m} - x_{1,k_m}|}\\
\delta_{x_{1,3},k} &= \sqrt[3]{|x_{3,k_m} - x_{1,k_m}|},
\end{aligned} \tag{24}$$

where $k \geq k_m$ refers to discrete time and k_m indicates the time instant when the last available values of the state variables arrived. The derived model shall predict the behavior of the building over certain prediction horizon during which no current values of the state variables are available. Therefore, at each "measurement" time instant, the values of $\delta_{x_{1,2},k}$ and $\delta_{x_{1,3},k}$ are calculated and they are used by the optimizer over the whole prediction horizon. The necessity of realizing the difference between the *real-life time* (in which the model is time-varying) and the *internal time of the optimizer* (in which the model stays constant over the prediction horizon) is obvious.

Then, the nonlinear terms appearing in the model Eq. (20) can be approximated as

$$\begin{aligned}
\sqrt[3]{|x_2 - x_1|}(x_2 - x_1) &\approx \delta_{x_{1,2},k}(x_{k_m})(x_2 - x_1),\\
\sqrt[3]{|x_3 - x_1|}(x_3 - x_1) &\approx \delta_{x_{1,3},k}(x_{k_m})(x_3 - x_1)
\end{aligned} \tag{25}$$

for all $k \geq k_m$. Here, the expressions $\delta_{x_{1,2},k}(x_{k_m})$, $\delta_{x_{1,3},k}(x_{k_m})$ are used to emphasize the fact that the values of auxiliary variables depend only on the last available state values.

The bilinear term in the last differential equation is (similar to the previous approaches) considered as the new controlled input q_{in} while the vector of disturbances d remains unchanged. The linearized difference equations can be now summarized as:

$$x_{k+1} = A_{app}(x_{k_m})x_k + B_{app}u_k + B_d d_k, \tag{26}$$

where

[1] Let us note that the parameters p_i of the discrete time model (20), $i \in \{1, 2, \ldots, 13\}$, differ from the parameters $\overline{p}_i$ of the continuous time model (19) since they incorporate also the effect of the chosen sampling period t_s.

$$A_{app}(x_{k_m}) = \begin{bmatrix} 1-(\tilde{p}_1+\tilde{p}_2+p_3) & \tilde{p}_1 & \tilde{p}_2 & 0 \\ \tilde{p}_5 & 1-(\tilde{p}_5+p_6+p_7) & p_6 & p_7 \\ \tilde{p}_8 & p_9 & 1-(\tilde{p}_8+p_9+p_{10}) & 0 \\ 0 & p_{12} & 0 & 1-p_{12} \end{bmatrix}, \quad (27)$$

with

$$\tilde{p}_1 = p_1\delta_{x_{1,2},k}, \quad \tilde{p}_2 = p_2\delta_{x_{1,3},k},$$
$$\tilde{p}_5 = p_5\delta_{x_{1,2},k}, \quad \tilde{p}_8 = p_8\delta_{x_{1,3},k} \quad (28)$$

and

$$B_{app} = \begin{bmatrix} 0 \\ 0 \\ 0 \\ p_{13} \end{bmatrix}, \quad B_d = \begin{bmatrix} p_3 & p_4 \\ 0 & 0 \\ p_{10} & p_{11} \\ 0 & 0 \end{bmatrix}. \quad (29)$$

At this point, the whole algorithm of obtaining the linear approximated model of the building can be summarized.

At each discrete sample $k = k_m$, the values of the state variables x are provided and the auxiliary variables $\delta_{x_{1,2},k}$, $\delta_{x_{1,3},k}$, are evaluated according to Eq. (24). Making use of the calculated auxiliary variables, a linear discrete-time model (26) of the building is created with the corresponding matrices. This approximated model is used until the new state values arrive, which means that at each discrete time sample, a new model is approximated and used by the optimizer over the following prediction horizon $k \in \{1, 2, \ldots, P\}$ of the *internal time of the optimizer*.

The readers interested in theoretical properties of the linear MPC exploiting model belonging to widely used family of linear time-/parameter-varying models (which SLM also belongs to) are warmly referred to Falcone, Borrelli, Tseng, Asgari, & Hrovat (2008) where the stability and feasibility of such formulation are discussed in detail. It should be noticed that one of the crucial assumption is that on constancy of the model over the prediction horizon, which is satisfied also by the SLM model and therefore, the results obtained in Falcone et al. (2008) hold also for the case of LMPC with SLM model.

3.4. MRI identification for nonlinear models

Having the model structures at disposal, it is necessary to estimate the parameters of these structures from the available input/output data. Since the obtained models are expected to be used by the predictive controllers as system dynamics predictors, this fact needs to be taken into account as early as at the point of choosing of the identification procedure. Instead of classical identification methods performing minimization of one-step prediction error (the so-called prediction error methods or PEMs Ljung, 2007), advanced approach focusing directly on minimization of multi-step prediction error is exploited since it provides models with better long-term prediction performance which is highly requested when considering use of the model with MPC. The objective is to find such parameters of the given model structure which minimize the multi-step prediction error (Laurí et al., 2010) over the whole prediction horizon,

$$J_{MRI} = \sum_{k=0}^{N-P}\sum_{i=1}^{P}\left[y_{k+i} - \hat{y}_{k+i|k}\right]^2, \quad (30)$$

where $\hat{y}_{k+i|k}$ is the i-step output prediction constructed from data up to time k, N corresponds to the number of samples and P stands for prediction horizon considered for identification. In case of linear model structures which is also the case of structure (22), several reliable approaches can be found. Therefore, one particular algorithm that has already been successfully used for building model parameters identification (interested readers are referred to Žáčeková & Prívara, 2012) will be used also in this paper to estimate the parameters of the linear structure (22).

When talking about identification of models with nonlinear structure performing minimization of (30), no methods of solving of the arisen problem can be found in the available literature according to authors' best knowledge. The proposed extension of the MRI identification methods (Žáčeková & Prívara, 2012) for nonlinear systems is described in the following text.

Without any loss of generality, let us assume nonlinear systems where the multi-step predictor $\hat{y}_{k+i|k}$ can be formulated in the following way:

$$\hat{y}_{k+i|k} = Z_{L,k+i}\hat{\theta}_L + Z_{NL,k+i}\hat{\theta}_{NL}, \quad i \in 1, 2, \ldots, P, \quad (31)$$

where $Z_{L,k+i} = [u_{k+i-n_d} \ldots u_{k+i-n_b}\, y_{k+i-1} \ldots y_{k+i-n_a}]$ and $\hat{\theta}_L = [\hat{b}_{n_d} \ldots \hat{b}_{n_b}\, \hat{a}_1 \ldots \hat{a}_{n_a}]$ are regression matrix and the vector of unknown parameters describing the linear part of the model dynamics, respectively. n_a denotes the number of past outputs in the regressor, n_b is the number of inputs in the regressor and n_d represents their delay compared to the outputs. The nonlinear part of the system dynamics is described by $\hat{\theta}_{NL} = [\hat{\theta}_1\ \hat{\theta}_2 \ldots \hat{\theta}_n]^T$ with n being the number of identified parameters and $Z_{NL,k+i} = [f_1(\cdot)\, f_2(\cdot) \ldots f_n(\cdot)]$.In general, $f_i(\cdot)$ are functions of $u_{k+i-1}, \ldots, u_{k+i-n_{b,NL}}$ and $y_{k+i-1}, \ldots, y_{k+i-n_{a,NL}}$ with parameters $n_{a,NL}$ specifying the number of past outputs in the nonlinear dynamics and $n_{b,NL}$ representing the number of inputs in the nonlinear structure.

It is important to note that not every output contained in regression matrices $Z_{L,k+i}$ and $Z_{NL,k+i}$ is available at time k, thus the multi-step predictions $\hat{y}_{k+i|k}$ must be obtained recursively by applying i-times the expression $\hat{y}_{k+1|k} = Z_{L,k+1}\hat{\theta}_L + Z_{NL,k+1}\hat{\theta}_{NL}$ with initial conditions y_k. Now, the estimate of matrix of parameters $\hat{\theta}$ can be obtained as a solution of the following optimization task:

$$[\hat{\theta}_L, \hat{\theta}_{NL}]^* = \arg\min_{[\theta_L,\theta_{NL}]} \sum_{i=1}^{P}\sum_{k=0}^{N-i} [y_{k+i} - Z_{L,k+i}\theta_L - Z_{NL,k+i}\theta_{NL}]^2$$

subject to :

$$\theta_L \in \theta_L(\mathcal{S}_L), \quad \theta_{NL} \in \theta_{NL}(\mathcal{S}_{NL}) \quad (32)$$

where $\mathcal{S}_L$ and $\mathcal{S}_{NL}$ correspond to the sets of all admissible estimated parameters. These constraints enable the user to incorporate certain a priori information into the identification procedure, for example to ensure that certain parameters are nonnegative or lie in a constrained interval, etc. In the currently presented case, two different methods of obtaining of $\hat{y}_{k+i|k}$ were exploited:

- *variant A* – for computing of $\hat{y}_{k+i|k}$, the output predictions are used only for recursive calculation of Z_L and for calculation of Z_{NL}, the available output data are exploited. In such case, the optimization task (32) is *polynomial* in parameters and can be solved employing standard solver for nonlinear programming. This is certain kind of approximation where the nonlinear part of the system dynamics is basically identified just in sense of minimization of one-step prediction error while the linear part is still identified with respect to the multi-step prediction error minimization criterion.
- *variant B* – for computing of $\hat{y}_{k+i|k}$, the output predictions are used for recursive calculation of Z_L as well as Z_{NL}. In this case, the parameters of both the linear and nonlinear part of the system dynamics are searched such that the multi-step prediction errors are minimized. It should be noted that in this case, the optimization task (32) is again a nonlinear programming problem, however, it might not be only polynomial in the estimated parameters any more.

3.5. Identification results

Making use of the above mentioned identification procedures, the parameters of all model structures presented in the current Section were identified from the available identification data set.

At first, the comparison of the nonlinear models obtained using variant A and variant B of the nonlinear MRI identification (denoted as nMRIa and nMRIb, respectively) is presented in Fig. 3. For identification purposes, prediction horizon $P=20$ samples was considered which with sampling period $t_s=15$ min corresponds to duration of 5 h. It can be argued that the prediction horizon is shorter than the real prediction horizon of the predictive controllers (in the current application, the predictive controllers perform optimization calculations over 12 h corresponding to 48 samples), however, in Žáčeková, Váňa, & Cigler (2014) and Gopaluni, Patwardhan, & Shah (2004) it was shown that from certain prediction horizon threshold, the increase of the identification prediction horizon can lead to degradation of the performance of the obtained model.

It is obvious that both obtained nonlinear models fit the verification data very well also on longer verification interval with slight superiority of the model identified making use of nMRIb. nMRIa variant provides model with performance which is only slightly worse than that of the model obtained by (seemingly) more computationally demanding variant nMRIb. It is true that within the nMRIb, a more general nonlinear programming task needs to be solved (which is undoubtedly more computationally demanding than just solving of polynomially nonlinear programming performed within nMRIa), however, the overall optimization which is solved within nMRIb takes less computational time than optimization performed within nMRIa. Although one iteration of nMRIb is slower (due to solving of the more general optimization problem), on the other hand less iterations are needed to converge to the solution of the optimization problem. This can be explained such that the task formulated within nMRIb brings the chosen nonlinear structure closer to reality and thus also to the verification data – this of course holds well only in case that a reasonable model structure was chosen. Therefore, it might be more advantageous to choose identification of nonlinear model in variant nMRIb which can be ultimately faster and provides a more accurate and reliable model. Based on this, the model obtained by nMRIb was chosen to be used with the nonlinear predictive controller in the role of the system dynamics predictor.

Now, the graphical and numerical comparison of all above described models follow. Since the models are intended to be used with the MPC, one of their most important features is the ability to provide reasonable predictions over the whole prediction horizon. In this paper, the prediction horizon T_P = 12 h is considered which with 15-min sampling corresponds to $P=48$ samples. Let us remind that in the role of the nonlinear model, nMRIb was chosen.

Fig. 4 shows several weeks of comparison of the models which are used for the building behavior predictions with the linear time invariant (LM model), linear time-varying (SLM model) and nonlinear MPC (NM model). At each discrete time sample ($t_s=15$ min), 12-h predictions are calculated based on the provided state values. All the predictions of the models are plotted together with the verification data.

Looking at Fig. 4, it is clear that while the NM behavior constraints the quality of the prediction behavior from above with the smallest deviations from the verification data and the LM behavior exhibits the highest prediction errors, the performance of the performance of the time-varying model is somewhere in the middle between these two “limit” cases. The most obvious are the differences in the behavior when looking at the 200-th and the 300-th hour of the comparison. While the absolute value of prediction errors for the off-line identified linear model reaches up to 2 °C, the error obviously decreases through the switched linearly approximated time-varying model down to the nonlinear model which provides the predictions with the least prediction error out of the three compared models, which in turn justifies the use of the predictive controller with the more complex nonlinear model.

In order to compare the models in a more complete way, the statistical comparison of the models is provided in Table 2. The length of the evaluated period was nearly 3 months. In the table, LM specifies the linear model, SLM stands for the switched linearly approximated model and NM represents the nonlinear model. For each model, ε_{av} being the average prediction error over the whole 12-h prediction horizon and the maximum prediction error ε_{max} over the prediction horizon are inspected.

The table clearly demonstrates that the most reliable predictions are provided by the NM model. However, this is not a surprise as this model takes the whole dynamics of the building into account including the nonlinearities. On the other hand, it can be seen that considering the linear time-dependent model, the quality of the predictions fairly improves compared to the linear time invariant model. With SLM model, the reduction of ε_{av} is almost 40% and the reduction of ε_{max} is nearly 37%.

4. Model predictive control

In this section, the considered MPC variants are briefly explained and the optimization routines used to solve the corresponding optimization problems are presented. At the end of this Section, the quantized nonlinear predictive control algorithm is proposed.

4.1. Linear MPC

The control requirements which have been chosen for the linear MPC to be satisfied (minimization of both the thermal comfort

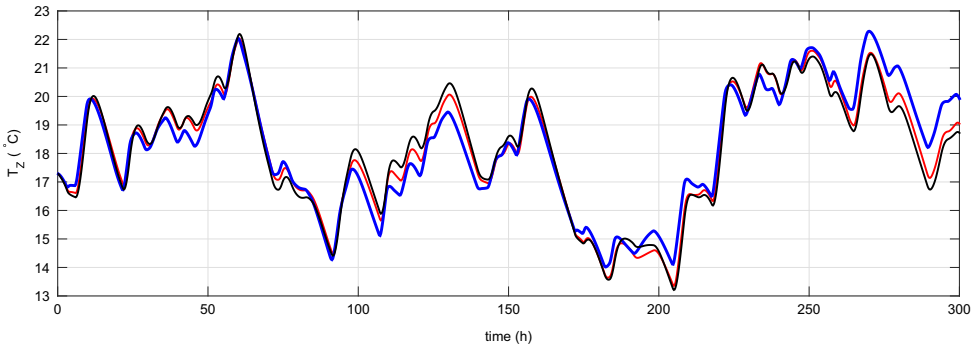

Fig. 3. Comparison of nMRIa (—) and nMRIb (—) models with the verification data (—).

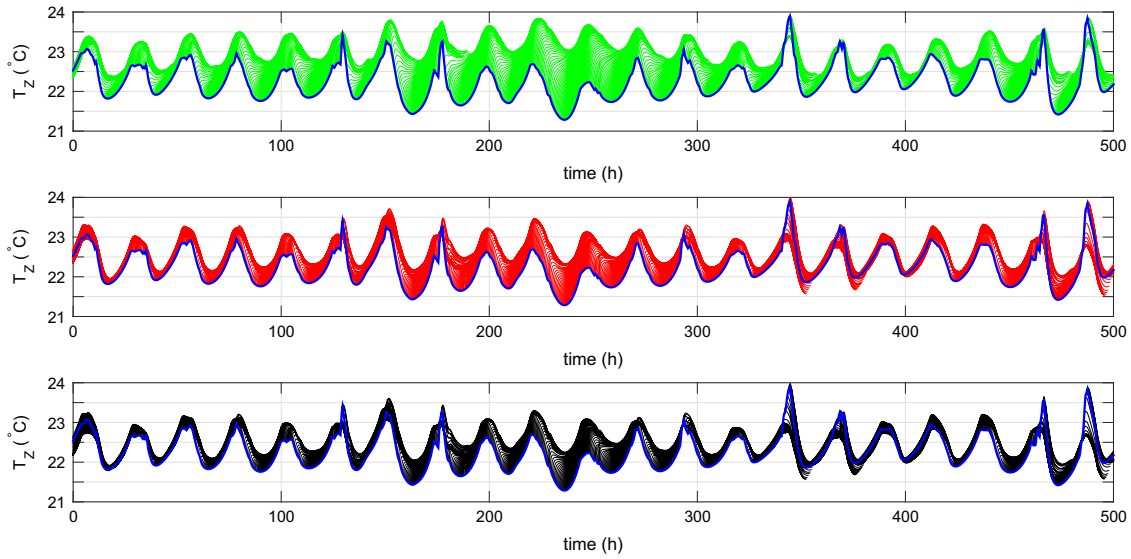

Fig. 4. Comparison of T_Z predictions of the LM (—), SLM (—) and NM (—) models with the verification data (—).

Table 2
Statistical comparison of the models.

	LM	SLM	NM
ε_{av} (°C)	0.57	0.34	0.30
ε_{max} (°C)	1.89	1.20	1.08

violation and the energy consumption) can be mathematically summarized as follows:

$$J_{MPC,k} = \sum_{i=1}^{P} W_{1,\mathbf{p}}(k+i) \| q_{\text{in},k+i} \|_{\mathbf{p}} + \sum_{i=1}^{P} W_{2,\mathbf{p}} \| CV_{k+i} \|_{\mathbf{p}} \tag{33}$$

$$\text{s. t.:} \quad \text{linear dynamics (22)}$$
$$0 \le q_{\text{in},k+i} \le \overline{q}_{\text{in},k+i}, \quad i = 1, \ldots, P$$
$$\hat{T}_{Z,k+i|k} \ge T_{Z,k+i}^{min} - CV_{k+i}.$$

This formulation considers a combination of linear and quadratic penalization indicated by the index $\mathbf{p} \in \{1, 2\}$ which enables us to shape the penalization criterion conveniently. Time-varying weighting matrices W reflecting the time dependence of the electricity tariffs and prediction horizon P stand for the tuning parameters of the controller. Comfort violation is calculated based on the difference between the zone temperature prediction $\hat{T}_Z$ and its lowest acceptable bound T_Z^{min} and the hard constraints are relaxed employing an auxiliary variable CV. Exact values of the optimization problem settings can be found in Table 3.

As the linear version of MPC optimizes supplied heat q_{in}, a post-processing procedure is needed to obtain the particular values of T_{SW} and $\dot{m}$ which correspond to the true control inputs of the thermally activated building system (TABS). This straightforward postprocessing holds the mass flow rate fixed $\dot{m} = \dot{m}_{pp}$ and it calculates the supply water command as $T_{SW} = q_{\text{in}}/\dot{m}c_w + T_R$. Should the calculated supply water command be higher than $\overline{T}_{SW}$, $T_{SW} = \overline{T}_{SW}$ is set and the mass flow rate command is calculated as $\dot{m} = q_{\text{in}}/c(T_{SW} - T_R)$. If the heating effort is lower than a threshold value $q_{\text{in},tr}$, the TABS manipulated variables are set to $T_{SW} = T_R$ and $\dot{m} = \underline{\dot{m}}$. The settings of the post-processing procedure are listed in Table 3.

Table 3
Table of controller parameters.

$W_{1,1}$ (high tariff)	0.01	$W_{1,2}$ (high tariff)	1.6
$W_{1,1}$ (low tariff)	0.005	$W_{1,2}$ (low tariff)	0.8
$W_{2,1}$	2×10^6	$\overline{q}_{\text{in}}$	90×10^4
$W_{2,2}$	10^4	$q_{\text{in},tr}$	700
$\underline{T}_{SW}$	20	$\overline{T}_{SW}$	50
P	48	$\dot{m}_{pp}$	20

4.2. Nonlinear MPC

Thanks to the use of nonlinear programming optimization method, the nonlinear MPC can exploit the more reliable nonlinear discrete-time state-space description of the building behavior and address directly the minimization of the evaluative criterion (6). To obtain computationally tractable solution, also the criterion (6) needs to be discretized in time. This results in the following nonlinear MPC cost criterion:

$$J_{NMPC,k} = \frac{1}{t_s}\sum_{i=1}^{P} \omega CV_{k+i} + \frac{1}{t_s}\sum_{i=1}^{P}\left(P_{E,k+i}(P_C(u_{2,k+i}) + P_C(\overline{u}_{3,k+i}))\right) + \frac{1}{t_s}\sum_{i=1}^{P} P_W \overline{u}_{3,k+i}, \tag{34}$$

where t_s represents the chosen constant sampling period, P stands for the prediction horizon, $P_C(\cdot)$ corresponds to Eq. (7) and $\overline{u}_3$ represents a virtual input which corresponds to the storage water mass flow rate $\dot{m}_{St}$,

$$\overline{u}_3 = u_2 \frac{u_1 - x_4}{T_{St} - x_4}.$$

The obtained optimal profiles u_1, u_2 are required to satisfy the technical limitations which are formulated as box constraints,

$$\max\{\underline{T}_{SW}, x_4\} \le u_{1,k} \le \overline{T}_{SW},$$
$$\underline{\dot{m}} \le u_{2,k} \le \overline{\dot{m}}. \tag{35}$$

Last but not least, the dynamics of the building must not be violated which is represented by the satisfaction of the model dynamics (20).

In the role of the optimization routine, gradient optimization algorithm (Zhou, Doyle, & Glover, 1996; Bryson, & Ho, 1975) with variable step length is employed. This approach is able to address optimization problems in the following form:

$$\text{minimize } J = \sum_{i=1}^{P} L(x_i, u_i) + \phi(x_P, u_P)$$
$$\text{such that } u_i \in \langle \underline{u}, \overline{u} \rangle. \tag{36}$$

To find the solution of (36), the following idea is employed: starting from an initial estimate of the optimal input profile u^0, the opposite direction of the gradient of the minimization cost criterion is iteratively followed until convergence to the optimal input vector,

$$u^l = u^{l-1} - \alpha^l \frac{\partial J}{\partial u}. \tag{37}$$

Here, l represents the iteration of the gradient algorithm and α^l is the step length at l-th iteration.

To obtain computationally tractable solution of this optimization task, the Hamiltonian

$$\mathcal{H} = L_k + \lambda_{k+1}^{\mathrm{T}} f(x_k, u_k) \tag{38}$$

is created. Here, L_k is the integral or in discrete-time case the *summation* part of the criterion J, $f(x_k, u_k)$ is the vector field representing the dynamics of the controlled system and λ is the so-called co-state vector with the backwards dynamics

$$\lambda_k = \frac{\partial H}{\partial x}(x_k, u_k, \lambda_{k+1}) \tag{39}$$

and the terminal condition

$$\lambda_P = \left.\frac{\partial J}{\partial x}\right|_P. \tag{40}$$

It can be shown that the gradients of both the cost criterion J and the Hamiltonian H with respect to the input vector u are equal, $\partial J/\partial u = \partial H/\partial u$, and therefore, the iterative search (37) turns into

$$u^l = u^{l-1} - \alpha^l \frac{\partial H}{\partial u}. \tag{41}$$

To satisfy the input constraints, the input profile u^l is at each iteration projected on the admissible input interval $\langle \underline{u}, \overline{u} \rangle$. The iterative search (41) is used until convergence which is usually defined as

$$|J(u^l) - J(u^{l-1})| \leq \epsilon \tag{42}$$

with some reasonably chosen nonnegative tolerance $\epsilon > 0$.

As can be expected, the search step length α significantly influences the convergence properties of the algorithm. In order to provide smooth and uniform convergence to the optimum, α should be small in case that the cost criterion J decreases rapidly and it should increase in case that the change of the cost criterion $|J(u^l) - J(u^{l-1})|$ is small. To satisfy these requirements, the following formula for the search step length is proposed:

$$\alpha^l = -\beta \log(\gamma \Delta J^l). \tag{43}$$

Here, $\Delta J^l = |J(u^l) - J(u^{l-1})|$ is the change of the cost function value and $\beta > 0$, $\gamma > 0$ are some suitably chosen constants. Last of all, the step length α^l is constrained at each gradient algorithm iteration,

$$\underline{\alpha} \leq \alpha^l \leq \overline{\alpha}. \tag{44}$$

Parameters $\underline{\alpha} > 0$ and $\overline{\alpha} > 0$ are together with β and γ considered to be the tuning parameters of the presented optimization algorithm.

4.3. Quantized MPC

As was mentioned earlier, the mass flow rate should belong to the admissible set of discrete values $\dot{M}_{\mathrm{adm}}$. In case of the linear MPCs which calculate optimal amount of energy that should be delivered into the zone and subsequently perform the postprocessing to obtain the values of mass flow rate and supply water temperature, the discrete-valued nature of the mass flow rate can be very straightforwardly taken into account. However, the situation is more complicated in case of nonlinear MPC. As already mentioned in the Introductory Section, two ways how to obtain discrete-valued mass flow rate sequence are considered in this work.

The first of them consists in use of additional postprocessing which is performed after the continuous-valued optimization is finished. The most straightforward postprocessing routine is pure rounding of the obtained continuous-valued mass flow rate sequence u_2 away from zero to the nearest multiple of the quantization step,

$$u_{2,q} = q_{st} \cdot \mathrm{round}\left(\frac{u_2}{q_{st}}\right), \tag{45}$$

with $\mathrm{round}(\cdot) = \mathrm{sgn}(\cdot)\lceil|\cdot|\rceil$. Major advantage of this approach is its simplicity – the a posteriori quantization can be performed by a hardware component and therefore, no increase of the computational complexity occurs. However, it can be expected that such naive approach significantly degrades the control performance of the original controller since the fact that the manipulated variable will be quantized a posteriori is not taken into account in the used optimization routine.

This drawback is solved by the adaptation of the original Hamiltonian-based method representing the second way of achieving that discrete-valued mass flow rate profile is obtained. Here, a regular *mid-processing* iteration is performed each **I**-th iteration of the gradient search. Thanks to this, the information about the discrete-valued nature of one of the manipulated variables is incorporated into the optimization procedure and the optimality of the original continuous-valued optimization technique is preserved.

The *mid-processing* is performed at particular iterations $l = m \times \mathbf{I}$, $m \in \mathbb{N}^+$ after the gradient step is made and it can be described as follows: first of all, the quantized mass flow rate sequence $u_{2,\bigcirc}^l$ is obtained by projecting the continuous-valued mass flow rate vector $\hat{u}_2^l$ on the admissible set $\dot{M}_{\mathrm{adm}}$ given by (8) with respect to the chosen quantization step q_{st},

$$u_{2,\bigcirc}^l = q_{st} \cdot \mathrm{round}\left(\frac{\hat{u}_2^l}{q_{st}}\right). \tag{46}$$

These P predicted quantized mass flow rate samples are connected with n_f past mass flow rate samples $\overleftarrow{u_2} = [u_{2,k-n_f}, u_{2,k-n_f-1}, \ldots, u_{2,k-1}]$ with k representing the current time step, and vector $\overleftrightarrow{U_2} = [\overleftarrow{u_2}, u_{2,\bigcirc}^l]$ is received. The vector $\overleftrightarrow{U_2}$ represents all mass flow rate samples that will have been applied into the system until time $k + P$ and have influence on the frequency properties of the manipulated variable u_2 .

Then, $\overleftrightarrow{U_2}$ is filtered with a suitably defined low-pass filter with order n_f which helps us to suppress the undesired high frequencies and decrease oscillations in the last P-sample subvector representing the currently optimized input sequence. This P-sample subvector is extracted and after quantization and projection on its admissible range is used for the next iteration of the gradient search.

The overall control algorithm is then summarized as follows:

Algorithm agqNPC

1. obtain current values of the state variables $x_{curr,k}$
2. consider input profiles from the previous iteration

$\{u_1^{l-1}, u_2^{l-1}\}$ and obtain state trajectories $X = [x_0, x_1, \ldots, x_P]$ according to the model (20) with $x_0 = x_{curr,k}$;

3. according to the co-state dynamics (39), obtain the co-state trajectory $\Lambda = [\lambda_0, \lambda_1, \ldots, \lambda_P]$ with terminal condition (40);
4. calculate gradients $\partial H/\partial u_1$, $\partial H/\partial u_2$, and perform gradient step (41), obtain ${u_1}^l$ and $\hat{u}_2^l$;
5. **if** $\mathrm{mod}(l, \mathbf{I}) = 0$
   then perform the *mid-processing*:
   (i) quantize mass flow rate $\hat{u}_2^l$ according to (46) with chosen q_{st}, obtain $u_{2,\bigcirc}^l$,
   (ii) create sequence $\overleftrightarrow{U}_2^l = [\overleftrightarrow{u}_2, u_{2,\bigcirc}^l]$,
   (iii) filter $\overleftrightarrow{U}_2^l$ using a low-pass filter of order n_f with the chosen characteristics, obtain $\overleftrightarrow{U}_{2,\mathrm{filt}}^l$,
   (iv) quantize $\overleftrightarrow{U}_{2,\mathrm{filt}}^l$ with chosen q_{st}, obtain $\overleftrightarrow{U}_{2,\mathrm{filt},\bigcirc}^l$,
   (v) extract ${u_2}^l$ as the last P samples of $\overleftrightarrow{U}_{2,\mathrm{filt},\bigcirc}^l$;
   else $u_2^l = \hat{u}_2^l$;
6. project the sequences ${u_1}^l$ and ${u_2}^l$ on the admissible intervals $\langle \max\{\underline{T}_{SW}, x_4\}, \overline{T}_{SW}\rangle$ and $\langle \underline{\dot{m}}, \overline{\dot{m}}\rangle$;
7. **if** $|J(\{u_1^l, u_2^l\}) - J(\{u_1^{l-\mathbf{I}}, u_1^{l-\mathbf{I}}\})| \leq \epsilon$
   then terminate,
   else $l = l + 1$, repeat from (2);
8. apply the first sample of the calculated input profiles into the system, in the next time instance repeat from (1).

The performance of both the naive a posteriori quantization and the algorithm employing the *mid-processing* iteration is verified in the following section. In order to provide a better comparison, the results of the original continuous-valued nonlinear MPC are provided together with the results of the linear versions of predictive controller.

5. Results

First of all, visual comparison of the thermal comfort performance is presented in Fig. 5.

Fig. 5 shows the zone temperature profiles over a 6-day period for the linear predictive controllers with LM and SLM and the nonlinear continuous-valued predictive controller. From this figure, it can be seen that all controllers are carefully tuned to achieve satisfactory thermal comfort performance since all of them are able to satisfy the room temperature requirements and maintain the zone temperature within the admissible zone above the zone temperature threshold. This feature is very crucial since a controller that does not fulfill the thermal comfort requirements and violates the zone temperature threshold significantly is literally useless for building temperature control. Out of all considered controllers, the nonlinear MPC (NMPC) exhibits the most superior performance – it satisfies the required thermal comfort keeping the zone temperature within the admissible range and on the other hand, it obviously does not waste too much energy keeping the zone temperature just as high above the threshold as needed. This result could have been expected as the NMPC combines the model with the best prediction performance out of the considered set and it also directly addresses the minimization of the optimization criterion corresponding to the ultimate evaluative performance criterion (6).

Fig. 6 provides the second part of the visual comparison – it depicts the monetary cost that is being paid for the control at each time instance.

All profiles exhibit sinusoidal-like trends – this is caused by the consideration of time-varying price of the electricity. The higher parts of the profiles correspond to low-tariff hours while the lower parts match the non-working hours with cheap electricity. Also from this figure, the monetarily more economical nature of the NMPC can be observed. The NMPC spares significant amount of expenses compared to its linear counterparts. This superiority comes from the use of more precise nonlinear model and it is of course caused also by the nonlinear cost function of the NMPC which directly corresponds to the amount of money that is paid for the control. It can be also seen that the SLM model which is closer to the nonlinear one enables also the controller with approximated cost function to achieve better economical performance than the original linear model. For further illustration, the cumulative sum of the monetary cost of the control is depicted in Fig. 7. The provided profiles are normalized with respect to the total price TP_{LM} that is paid by the linear MPC with the ordinary time-invariant linear model.

The statistical comparison of the energy consumption can be found in Table 4. *TP* expresses the overall price paid for zone temperature control. Moreover, the particular energy consumptions normalized with respect to the consumption of the linear MPC using the ordinary off-line identified linear model are expressed. Furthermore, also the comparison of the average computational time T_{av} and the maximum computational time T_{max} per discrete time instance is provided.

The superiority of the NMPC is demonstrated once again. It can be seen that although the comparison of the identified models was very optimistic in the case of linear time-dependent model versus the linear time-invariant one, the resulting effect of the good

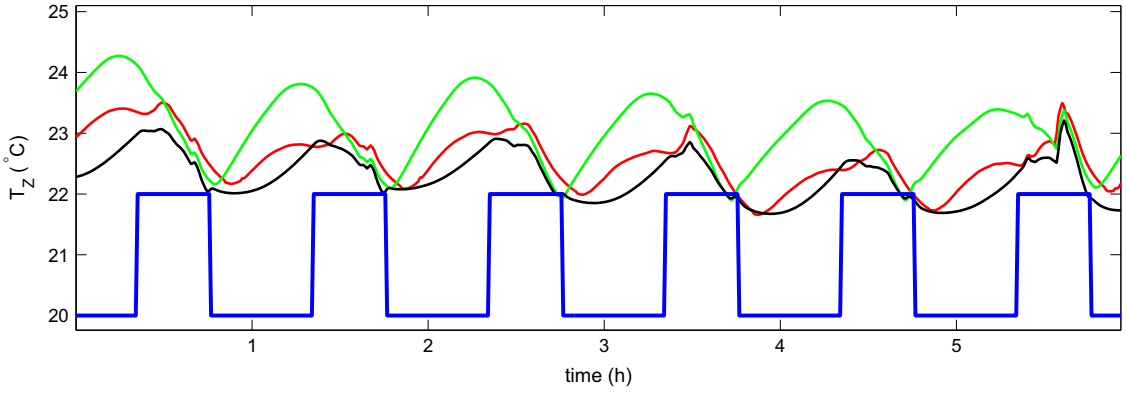

Fig. 5. Zone temperature control (– linear MPC with LM, – linear MPC with SLM, – nonlinear continuous-valued MPC with NM, – T_Z^{min}).

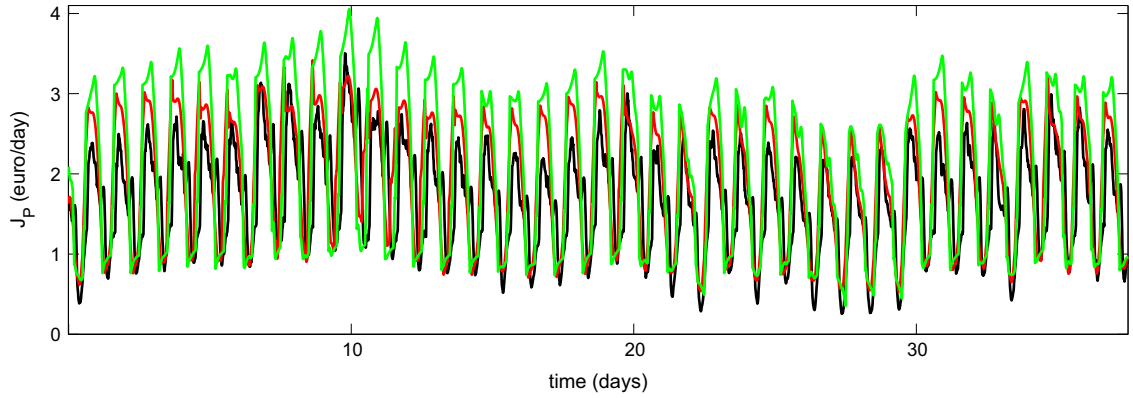

Fig. 6. Overal price of the control effort (— – linear MPC with LM, — – linear MPC with SLM, — – nonlinear continuous-valued MPC with NM).

model on the overall monetary cost of the control is not so attractive. This can be simply explained by the fact that although the good predictor is crucial for the proper functioning of the MPC (either linear or nonlinear), so is the properly chosen optimization criterion. Based on this observation, in the building climate control, the need for the use of nonlinear MPCs which are able to address the task of the real-life price minimization in a direct way instead of using certain approximation is obvious. However, one more aspect needs to be taken into account when choosing the controller type – its computational complexity. Table 4 shows two factors related to the computational demands of the particular control strategy: T_{av} being the average computational time needed for the calculation of the optimal input and T_{max} corresponding to the maximum calculation time. Let us mention that this calculation time includes also the time needed to obtain the model which (as will be shown) might contribute considerably to the overall calculation time. The comparison is evaluated depending on the type of the model which is used by the optimizer. The simplest controller being the LMPC with LM needs the shortest time to calculate the optimal input. As this variant does not consume any time to obtain the model and the same optimizer is used also by second member of the family of the linear MPCs (the controller with SLM model), one can get a very good insight into how long does it take to obtain the SLM model for the predictions. As the SLM variant performs the approximation of the nonlinear model at each sampling instant, the increase of the average computational time is understandable. Although in case of the LMPC with SLM, the average calculation time is longer than in case of the LMPC with LM, this is compensated by the better control performance.

Let us summarize the performance of the particular variants. Regarding the control performance and the energy consumption, the NMPC is the best candidate for the real-life application. On the other hand, the LMPC with the simplest off-line identified model is able to provide the fastest calculation of the optimal input sequence. Looking for a trade-off between the optimality and the time complexity, the presented time-varying approach exploiting SLM model is able to bridge the gap between these two and therefore, it stands for a promising candidate for the real-life application especially in case of large buildings complexes where it can be expected that the nonlinear optimization task can take too long to be solved.

Table 4
Comparison of the energy consumption and computational complexity.

	LM	SLM	NM
TP	83.7	77.0	66.8
TP/TP_{LM} (%)	100	92	80
T_{av} (s)	0.81	0.93	4.41
T_{max} (s)	1.20	1.49	6.21

Since one of the main objectives of this paper was to adapt the nonlinear MPC such that it provided discrete-valued mass flow rate profile, let us present a comparison of the performance of the following alternatives – the naive a posteriori quantization that is referred to as nqNPC and the adaptation of the gradient algorithm named agqNPC are compared with the continuous-valued NMPC from the previous comparison. At first, the situation with 7 admissible values for mass flow rate was considered. All three compared controllers (continuous-valued NMPC, nqNPC and agqNPC) were tuned to achieve approximately the same thermal comfort and therefore, only the economical part of the criterion might be focused on. At first, the calculated mass flow rate profiles are presented in Fig. 8.

Based on the visual comparison, it can be expected that the

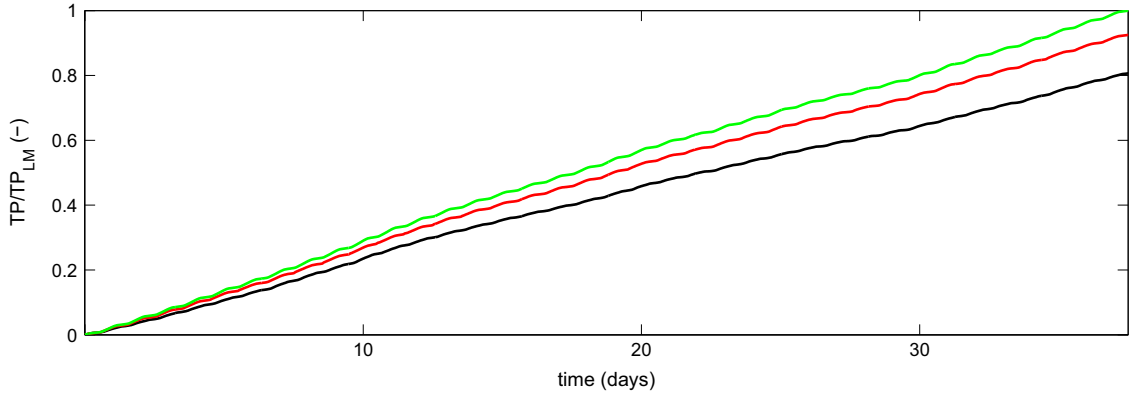

Fig. 7. Normalized cumulative price of the control effort (— – controller with LM , — – controller with SLM, — – controller with NM).

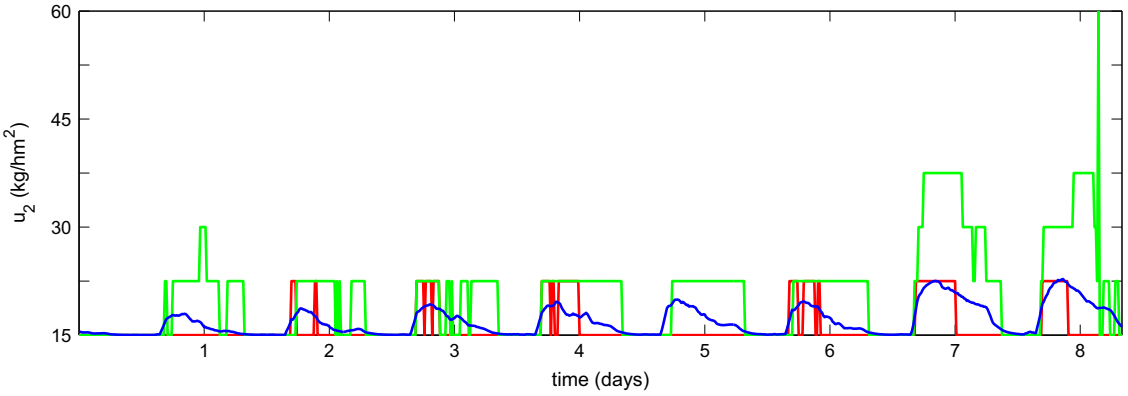

Fig. 8. Mass flow rates, $N_{qst} = 7$ (– continuous-valued NMPC, – nqNPC, – agqNPC).

nqNPC pays the most for the operation of the building. On the other hand, the agqNPC with advanced handling of the quantization phenomena behaves more similar to the original continuous-valued NMPC. This demonstrates the fact that while within the agqNPC, the mid-processing iteration enables us to adapt the calculation of the mass flow rate *inside* the optimization procedure and take the quantization into account, the naive quantization does not provide such possibility and therefore, significant part of the optimality is lost. Moreover, a posteriori quantization obviously leads to more oscillatory profiles which stands for another drawback of such approach. Since the mass flow rate is not the only manipulated variable, it might be interesting to inspect how much affected is u_1 by the quantization of u_2. Such comparison is provided in Fig. 9 where the profiles of supply water temperature applied by the inspected controllers are shown.

Comparing Figs. 8 and 9, a waterbed effect of the quantization can be observed since the quantization of one manipulated variable causes oscillatory performance that "leaks" into the other manipulated variable profile. The situation might seem a little bit paradoxically – although the mass flow rate is the manipulated variable that is quantized, the other manipulated variable also strongly oscillates when comparing the quantized version with the original continuous-valued version of the controller. This is more significant in case of the nqNPC where the oscillations of the supply water temperature are much more aggressive than the oscillations of the mass flow rate. This can be explained by the fact that while the quantization of the mass flow rate projects the values belonging to particular interval to the same quantized value, no such "damping" applies to the supply water temperature and therefore, its oscillations fully develop.

The last part of the comparison is the numerical evaluation of the economical aspects of the control under the quantization conditions provided in Table 5. Besides the total control cost (denoted as NMPC, nqNPC and agqNPC according to the evaluated control algorithm) shown in euros, also percentage increases of energy consumption normalized with respect to the consumption achieved by continuous-valued NMPC are provided (in Table 5, the increases are referred to as EI_{nqNPC} and EI_{agqNPC}, respectively). To obtain a more reliable comparison, situations with 3 up to 8 quantization steps N_{qst} were compared. The range of quantization levels $N_{qst} \in \{3, \ldots, 8\}$ was chosen based on the actual market research – it turned out that none of the currently available water pumps offers use of more than 8 pre-programmed different speeds/mass flow rates and therefore, values of N_{qst} higher than 8 were not considered. On the other hand, the theory of optimal bang-bang (2-valued) control is nearly as mature and elaborated as the optimal control theory itself (Anderson & Moore, 1971; Kaya & Noakes, 1996; Ledzewicz & Schättler, 2002; Wonham & Johnson, 1964) – therefore the optimization problem with 2-valued valve was omitted and the lowest number of quantization levels was chosen as $\underline{N}_{qst} = 3$.

Inspecting Table 5, it is obvious that the increase of the quantization steps N_{qst} leads to decrease of the cost paid for the control – this holds for both the naive and advanced quantization handling. However, a considerable difference can be observed in the actual value of the control cost increase. While for the naive quantization algorithm nqNPC the control cost can be increased by as high portion as 28%, the control cost increase never exceeds 17% with the use of advanced agqNPC algorithm. The difference can be nicely illustrated on an example of $N_{qst} = 4$ steps. The advanced quantization algorithm agqNPC consumes only about 10% more energy than the continuous-valued NMPC while the naive quantization algorithm nqNPC cost increase is nearly twice as high – moreover, even with $N_{qst} = 6$ quantization steps, the nqNPC algorithm achieves worse control cost. The difference between the two algorithms turns

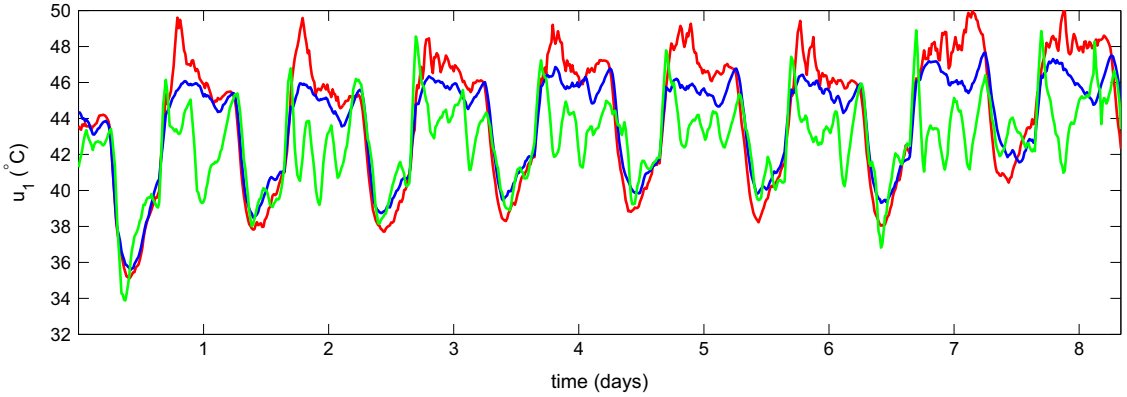

Fig. 9. Supply water temperatures, $N_{qst} = 7$ (– continuous-valued NMPC, – nqNPC, – agqNPC).

Table 5
Comparison of the energy cost.

N_{qst}	NMPC	nqNPC	EI_{nqNPC}	agqNPC	EI_{agqNPC}
3	66.8	85.6	28.1	78.1	17.0
4	66.8	80.2	20.1	73.6	10.2
5	66.8	76.1	13.9	72.5	8.5
6	66.8	75.2	12.6	69.0	3.3
7	66.8	72.4	8.3	67.6	1.2
8	66.8	67.5	1.0	67.1	0.4

insignificant only for the highest number of quantization steps $N_{qst} = 8$. However, although the control cost increase might not be significant, the difference in handling the oscillatory effects should not be forgotten as documented in Fig. 10 which clearly shows that the high-frequency portion of both the mass flow rate and the supply water temperature signals is decreased by the agqNPC and brought closer to the continuous-valued NMPC.

Last but not least, the computational complexity should be mentioned. Since the naive quantization algorithm nqNPC involves only a post-processing procedure to handle the quantization, virtually no computational time increase compared with the continuous-valued NMPC is observed. In case of the advanced quantization algorithm agqNPC, the *mid-processing* iteration causes a constant average increase of the computational complexity $\Delta_{ct} = 0.28$ s representing about 6% of the average computational time of the continuous-valued NMPC. Here, it should be highlighted that the computational complexity increase introduced by the use of the agqNPC is *independent* of the number of quantization levels N_{qst} which strongly distinguishes it from the commonly used mixed-integer programming methods where the computational time rises very steeply even when using massive computational power (Causa et al., 2008; Geyer, Larsson, & Morari, 2003; Lenstra, 1983; Pancanti et al., 2002).

Given the combination of less oscillatory and more economical performance (compared with the naive quantization) and constant trifling time complexity increase, it can be concluded that the agqNPC is the better and more attractive choice for the industrial application of control with discrete-valued input variables.

6. Conclusion

The task of advanced building climate control was formulated, several ways how to solve it using model based predictive control paradigm (namely linear MPC with ordinary linear model, nonlinear MPC and linear MPC with time-varying linear model) were presented and chosen practically oriented aspects were discussed in this paper.

Since the modeling and the estimation of the unknown parameters of the model structures is crucial for proper functionality of the predictive controller, the first part of the paper was devoted to the related problems. MRI method that is known to be the appropriate choice for the identification for predictive controllers with linear model was used for identification of the linear model structure and furthermore, it was adapted for use in case of nonlinear model structures. With both presented variants of the nonlinear MRI algorithm, models with good prediction properties were obtained. Furthermore, a bridge between the nonlinear and linear model structure was introduced by a switched linear approximated model (SLM). All identified models (linear model, nonlinear model and SLM model) were tested on a series of verification data and the achieved results certified them for use within the MPC scheme.

The next part of the paper covers the design of the predictive controller. The algorithm for both linear and the nonlinear MPC were provided. According to the specifications of the control systems presented in the Introductory Section, one of the manipulated variables might not be set with infinite resolution. Therefore, certain adaptations of the predictive controllers were necessary. For the linear MPCs, the adaptation consisted only in change of admissible post-processing values for mass flow rate and therefore, it was not discussed in the paper. However, the adaptation of nonlinear MPC was more delicate. Out of the three possible options (use of mixed-integer programming, naive a posteriori quantization and inclusion of mid-processing iteration into the optimization routine), the first one was abandoned due to its high computational requirements. While the naive a posteriori quantization represents only another post-processing procedure, the last option with the mid-processing iteration of the optimization algorithm adapts the original continuous-valued optimization and incorporates the information about the quantization directly into the optimization routine.

All the presented controllers were compared with respect to the pre-defined evaluative criterion based on the real-life requirements and costs. The results demonstrate that although the nonlinear continuous-valued predictive controller addresses the minimization of the given evaluative criterion in the best way, it was also quite time consuming. Therefore, the linear MPC exploiting the SLM model can be regarded as a reasonable trade-off between the optimality of the solution and the time complexity of the underlying optimization, especially in case of huge centrally-controlled building complexes where the complexity of the optimization task can be very high.

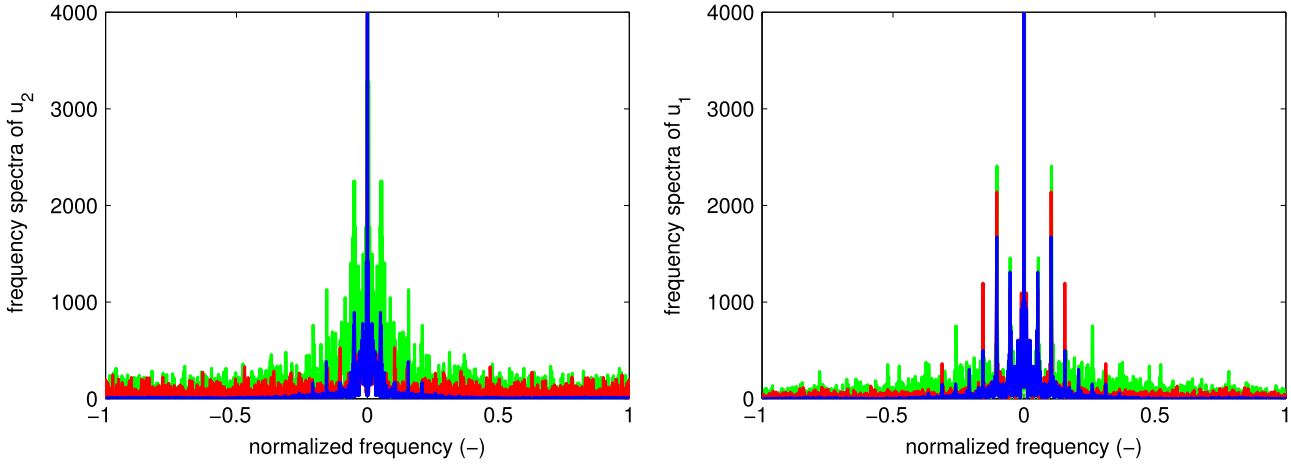

Fig. 10. Frequency spectra of the optimized variables, $N_{qst} = 8$ (– continuous-valued NMPC, – nqNPC, – agqNPC).

The other part of the comparison was focused on evaluation of the performance of the nonlinear controllers under the restrictions on the discrete-valued nature of the mass flow rate. The provided comparison shows that the advanced of the inspected methods agqNPC is not only able to keep the economical aspects of the control closer to standard of the original continuous-valued controllers but also helps us to reduce the oscillations of the manipulated variables for the cost of a negligible *constant* time complexity increase. Therefore, it can be suggested that the advanced agqNPC algorithm be used in practice instead of naive but commonly frequently used a posteriori quantization.

Regarding the future work, it would be interesting to examine the effect of incorporation of the persistent excitation condition into the predictive controller procedure. Based on the available literature, if the persistent excitation condition is included, more informative data are obtained which then turns into a better ability to estimate the model parameters accurately. The suggested procedure should be compared with the advanced Kalman filtering algorithms such as Extended or Unscented Kalman filtering. Moreover, a procedure for the model parameter update should be designed for the nonlinear model. Last but not least, based on the performed numerical experiments the authors suggest the strategies be tested on a building in real operation.

Acknowledgment

This research has been supported by the Czech Science Foundation through the Grant nos. 13-20433S and 13-12726J.

References

Anderson, B. D. & Moore, J. B. (1971). *Linear optimal control* (Vol. 197). Englewood Cliffs: Prentice-Hall.

ASHRAE. (2009). *ASHRAE-handbook fundamentals*. NE Atlanta, GA: American society of heating, refrigerating and air-conditioning engineers, Inc.

Balmer, R. T. (2010). *Modern engineering thermodynamics-textbook with tables booklet*. Academic Press, Oxford, UK.

Barták, M. (2010). *Úvod do přenosových jevu pro inteligentní budovy*. Prague, Czech Republic: CTU Prague.

Bryson, A. E., & Ho, Y. C. (1975). *Applied optimal control: optimization, estimation, and control*. Taylor and Francis, Oxford, UK.

Bussieck, M. R. & Vigerske, S. (2010). MINLP solver software. In *Wiley encyclopedia of operations research and management science*.

Causa, J., Karer, G., Núnez, A., Sáez, D., Škrjanc, I., & Zupančič, B. (2008). Hybrid fuzzy predictive control based on genetic algorithms for the temperature control of a batch reactor. *Computers & Chemical Engineering*, *32*(12), 3254–3263.

Chi, Q., Fei, Z., Zhao, Z., Zhao, L., & Liang, J. (2014). A model predictive control approach with relevant identification in dynamic PLS framework. *Control Engineering Practice*, *22*, 181–193.

European Economic and Social Committee. (2005). S.M. act: Communication from the commission to the council, The European parliament, The European economic and social committee and the committee of the regions.

Falcone, P., Borrelli, F., Tseng, H. E., Asgari, J., & Hrovat, D. (2008). Linear time-varying model predictive control and its application to active steering systems: *Stability analysis and experimental validation*. *International Journal of Robust and Nonlinear Control*, *18*(8).

Geyer, T., Larsson, M., & Morari, M. (2003). Hybrid emergency voltage control in power systems. In *Proceedings of the European control conference*, 2003.

Gopaluni, R., Patwardhan, R., & Shah, S. (2004). MPC relevant identification—Tuning the noise model. *Journal of Process Control*, *14*(6), 699–714.

Gyalistras, D., & Gwerder, M. (2010). Use of weather and occupancy forecasts for optimal building climate control (OptiControl): Two years progress report. Terrestrial Systems Ecology ETH Zurich, Switzerland and Building Technologies Division, Siemens Switzerland Ltd., Zug, Switzerland.

Kaya, C. Y., & Noakes, J. L. (1996). Computations and time-optimal controls. *Optimal Control Applications and Methods*, *17*(3), 171–185.

Laurí, D., Salcedo, J., Garcia-Nieto, S., & Martínez, M. (2010). Model predictive control relevant identification: *Multiple input multiple output against multiple input single output*. *Control Theory & Applications, IET*, *4*(9).

Ledzewicz, U., & Schättler, H. (2002). Optimal bang–bang controls for a two-compartment model in cancer chemotherapy. *Journal of Optimization Theory and Applications*, *114*(3), 609–637.

Lenstra, H. W., Jr. (1983). Integer programming with a fixed number of variables. *Mathematics of Operations Research*, *8*(4), 538–548.

Lienhard, J. H. (2013). *A heat transfer textbook*. Courier Corporation, Cambridge, Massachusetts, USA.

Ljung, L. (1999). *System identification*. Wiley Online Library.

Ljung, L. (2007). System identification toolbox for use with {MATLAB}.

Ma, J., Qin, S. J., Li, B., & Salsbury, T. (2011). Economic model predictive control for building energy systems. In *2011 IEEE PES innovative smart grid technologies (ISGT)* (pp. 1–6). IEEE, Piscataway, NJ, USA.

Ma, Y., Kelman, A., Daly, A., & Borrelli, F. (2012). Predictive control for energy efficient buildings with thermal storage: *Modeling, stimulation, and experiments*. *IEEE Control Systems, Magazine*, *32*(1), 44–64.

Oldewurtel, F., Gyalistras, D., Gwerder, M., Jones, C., Parisio, A., Stauch, V., et al. (2010). Increasing energy efficiency in building climate control using weather forecasts and model predictive control. In *10th REHVA world congress clima* (pp. 9–12).

Pancanti, S., Leonardi, L., Pallottino, L., & Bicchi, A. (2002). Optimal control of quantized input systems. In *Hybrid systems: computation and control* (pp. 351–363). Springer, Berlin Heidelberg, Germany.

Perez-Lombard, L., Ortiz, J., & Pout, C. (2008). A review on buildings energy consumption information. *Energy and Buildings*, *40*(3), 394–398.

Prívara, S., Široký, J., Ferkl, L., & Cigler, J. (2011). Model predictive control of a building heating system: *The first experience*. *Energy and Buildings*, *43*(2), 564–572.

Pčolka, M., Žáčeková, E., Robinett, R., Čelikovský, S., & Šebek, M. (2014). Economical nonlinear model predictive control for building climate control. In *American control conference (ACC), 2014* (pp. 418–423). IEEE, Piscataway, NJ, USA.

Pčolka, M., Žáčeková, E., Robinett, R., Čelikovský, S., & Šebek, M. (2014). From linear to nonlinear model predictive control of a building. In *IFAC world congress 2014* (Vol. 19, pp. 587–592).

R.O. for Network Industries. (2011). Approved electricity tariffs for the household consumers for 2011 (online). ⟨http://www.urso.gov.sk/doc/dokumenty/PorovnanieMaxCienEEpreDomacnisti2011.pdf⟩, accessed: 03/11/2013.

Shook, D. S., Mohtadi, C., & Shah, S. L. (1991). Identification for long-range predictive control. In *IEEE proceedings D (Control theory and applications)* (Vol. 138, pp. 75–84). IET, Piscataway, NJ, USA.

Stetter, H. J. (1973). *Analysis of discretization methods for ordinary differential equations* (Vol. 23). Springer, Berlin Heidelberg, Germany.

University of Wisconsin-Madison, Solar Energy Laboratory, & Klein, S. A. (1979). *TRNSYS, a transient system simulation program*. Solar Energy Laboratory, University of Wisconsin–Madison.

Verhelst, C., Degrauwe, D., Logist, F., Van-Impe, J., & Helsen, L. (2012). Multi-objective optimal control of an air-to-water heat pump for residential heating. *Building Simulation*, *5*, 281–291.

Wonham, W. M., & Johnson, C. (1964). Optimal bang–bang control with quadratic performance index. *Journal of Fluids Engineering*, *86*(1), 107–115.

Žáčeková, E., & Prívara, S. (2012). Control relevant identification and predictive control of a building. In *2012 24th Chinese control and decision conference (CCDC)* (pp. 246–251). IEEE, Piscataway, NJ, USA.

Žáčeková, E., Váňa, Z., & Cigler, J. (2014). Towards the real-life implementation of MPC for an office building: *Identification issues*. *Applied Energy*, *135*, 53–62.

Zhao, J., Zhu, Y., & Patwardhan, R. (2014). Some notes on MPC relevant identification. In *American control conference (ACC), 2014* (pp. 3680–3685). IEEE, Piscataway, NJ, USA.

Zhou, K., Doyle, J. C., Glover, K., (1996). *Robust and optimal control* (Vol. 40). New Jersey: Prentice Hall, Upper Saddle River, New Jersey, USA.

Zmrhal, V., & Drkal, F. (2006). The influence of heat convection on room air temperature. In *Proceedings of 17th air-conditioning and ventilation conference*.